


SuperSpec, The On-Chip Spectrometer: Improved NEP and Antenna Performance

Jordan Wheeler¹  · S. Hailey-Dunsheath² · E. Shirokoff³ · P. S. Barry^{3,4} · C. M. Bradford^{2,5} · S. Chapman⁶ · G. Che⁷ · S. Doyle⁴ · J. Glenn¹ · S. Gordon⁷ · M. Hollister² · A. Kovács² · H. G. LeDuc⁵ · P. Mauskopf⁷ · R. McGeehan³ · C. McKenney⁸ · T. Reck⁴ · J. Redford² · C. Ross⁶ · C. Shiu² · C. Tucker⁴ · J. Turner⁹ · S. Walker¹ · J. Zmuidzinas^{2,5}

Received: 19 October 2017 / Accepted: 16 April 2018 / Published online: 4 May 2018
© Springer Science+Business Media, LLC, part of Springer Nature 2018

Abstract SuperSpec is a new technology for mm and sub-mm spectroscopy. It is an on-chip spectrometer being developed for multi-object, moderate-resolution ($R \sim 300$), large bandwidth survey spectroscopy of high-redshift galaxies for the 1 mm atmospheric window. This band accesses the CO ladder in the redshift range of $z = 0\text{--}4$ and the [CII] $158\ \mu\text{m}$ line from redshift $z = 5\text{--}9$. SuperSpec employs a novel architecture in which detectors are coupled to a series of resonant filters along a single microwave feedline instead of using dispersive optics. This construction allows for the creation of a full spectrometer occupying only $\sim 10\ \text{cm}^2$ of silicon, a reduction in size of several orders of magnitude when compared to standard grating spectrometers. This small profile enables the production of future multi-beam spectroscopic instruments

✉ Jordan Wheeler
Wheeler1711@gmail.com

¹ Center for Astrophysics and Space Astronomy, University of Colorado, Boulder, CO 80309, USA

² California Institute of Technology, 1200 E. California Blvd, Mail Code 301-17, Pasadena 91125, USA

³ Department of Astronomy and Astrophysics, University of Chicago, 5640 South Ellis Avenue, Chicago, IL 60637, USA

⁴ School of Physics and Astronomy, Cardiff University, 5 The Parade, Cardiff CF24 3AA, UK

⁵ Jet Propulsion Laboratory, 4800 Oak Grove Drive, Pasadena, CA 91109, USA

⁶ Department of Physics and Atmospheric Science, Dalhousie University, Coburg Road, Halifax, NS B3H 1A6, Canada

⁷ Department of Physics, School of Earth and Space Exploration, Arizona State University, Tempe, AZ 85287, USA

⁸ National Institute of Standards and Technology, 325 Broadway, Boulder, CO 80305, USA

⁹ Department of Physics and Astronomy, University of Wyoming, 1000 E. University, Laramie, WY 82071, USA

envisioned for the millimeter band to measure the redshifts of dusty galaxies efficiently. The SuperSpec collaboration is currently pushing toward the deployment of a SuperSpec demonstration instrument in fall of 2018. The progress with the latest SuperSpec prototype devices is presented; reporting increased responsivity via a reduced inductor volume ($2.6 \mu\text{m}^3$) and the incorporation of a new broadband antenna. A detector NEP of $3\text{--}4 \times 10^{-18} \text{ W/Hz}^{0.5}$ is obtained, sufficient for background-limited observation on mountaintop sites. In addition, beam maps and efficiency measurements of a new wide-band dual bow-tie slot antenna are shown.

Keywords Spectrometer · Kinetic inductance detectors · NEP · Bow tie · Antenna · mm-wave

1 Introduction

SuperSpec is a new mm/sub-mm spectrometer technology [1–6]. It is an on-chip filterbank being developed for multi-object, moderate-resolution ($R \sim 300$), large bandwidth survey spectroscopy of high-redshift galaxies. In particular, the current SuperSpec design targets the CO ladder in the redshift range of $z = 0\text{--}4$ and the [CII] $158 \mu\text{m}$ line from redshift $z = 5\text{--}9$. SuperSpec's small footprint enables future sub-mm and mm instruments by allowing many spectrometers to be packed into a single focal plane, a necessary requirement to observe a large statistical sample of high-redshift galaxies. The SuperSpec technology can also be applied to cosmological science through tomographic mapping of cumulative emission of spectral lines (e.g., Time Pilot [7]) using many spectrometers in a single focal plane (an integral field unit) to build up a 3D (2 spatial and 1 spectral) data cube. The power spectrum of this data cube can be used to statistically constrain cosmological structure formation models.

SuperSpec receives astrophysical radiation via a lens-coupled antenna. This radiation propagates down a microstrip transmission line where specific frequencies of radiation are picked off by proximity-coupled, half-wavelength microstrip resonators. Careful tuning of the proximity of the resonators to the feedline dials in the desired resolving power of the SuperSpec filterbank by tuning the coupling quality factor. The half-wavelength resonators are coupled in turn to the inductive meander of kinetic inductance detectors (KIDs), which serve as the power detectors for the SuperSpec filterbank as shown in Fig. 1. Each SuperSpec filterbank contains hundreds of KIDs, and the KIDs' high-quality factors allow for the readout of large numbers of detectors. The unique coupling scheme employed by SuperSpec allows for the creation of incredibly low volume, high responsivity, titanium nitride (TiN) KIDs: current inductor volumes are $2.6 \mu\text{m}^3$. Since responsivity is proportional to the inverse of quasiparticle-occupied volume, this allows SuperSpec to reach the low NEPs required by moderate-resolution spectroscopy to be photon-limited from the best ground-based observing sites, i.e., $5 \times 10^{-18} \text{ W/Hz}^{0.5}$ at $R = 300$.

This paper presents results from three of our 50-channel prototype filterbank devices. Devices come from two wafers, both fabricated in the same run in the JPL Micro Devices Lab (MDL). Device 1 was derived from one wafer, and Devices 2A and 2B were derived from the second wafer. Devices 1 and 2A were tested optically, while

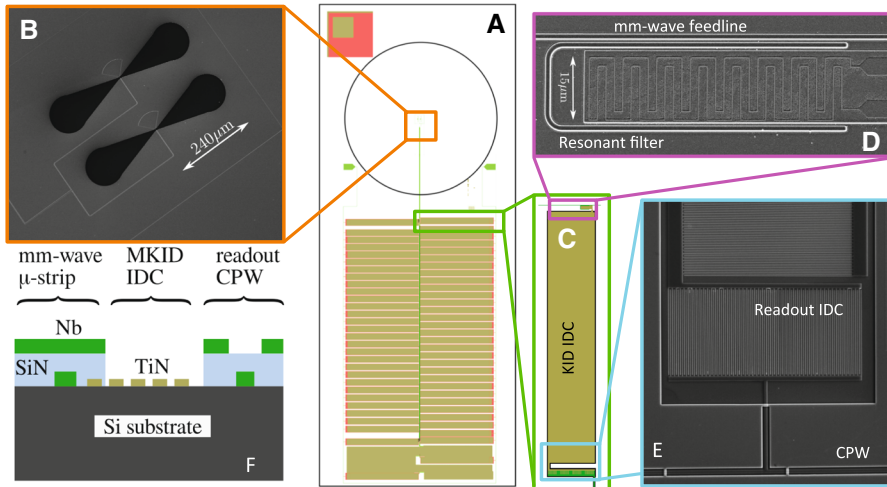


Fig. 1 SuperSpec test device. **a** A mask with dual bow-tie slot antenna and lens footprint at the top, and feedline running vertically past an array of band-pass filters. **b** Dual bow-tie slot antenna. **c** A single mm-wave filter and KID (KID resonant frequencies are from ~ 100 – 200 MHz). **d** The mm-wave resonator and 250-nm line width inductor. **e** The lower portion of the large interdigitated capacitor (IDC), coupling IDC, and readout coplanar waveguide. **f** Cross section showing the device layers. (Color figure online)

2B was tested dark in a light-tight box. In this paper, two important developments of the SuperSpec prototype devices are discussed: increased responsivity detectors via reducing detector inductor volume and the incorporation of a new broadband antenna.

2 Detector Responsivities, Noise, and NEP

To improve the SuperSpec KID sensitivity, a new ultra-low-volume inductor utilizing 0.25-micron-wide lines patterned in 20-nm TiN film has been developed. The total inductor volume is $2.6 \mu\text{m}^3$, and these inductors are produced with high yield. Fractional frequency response to optical loads is calibrated in the usual way using nitrogen-cooled loads relative to ambient. Additionally, a concave mirror outside the cryostat is utilized to achieve an effective temperature of ~ 15 K, less than expected at the observatory (30–60 K).

The frequency responsivity is obtained from the slope of the photon noise as a function of loading when excited by a coherent local oscillator source. The change in photon noise as a function of the change in power is related to the responsivity, R , via $dS_{xx}/dP = 4R^2 h\nu$, where $dP = (\Delta f/f)/R = dx/R$, when loaded using a coherent source which produces purely shot noise [2]. This assumes that the responsivity is constant with changing loading, which has been confirmed for these TiN detectors over the power level range used for this measurement, and is further confirmed by the linearity of the data in Fig. 2 left.

For Device 1, a responsivity of $1.4 \times 10^{10} \text{ W}^{-1}$ (Fig. 2 left) is found along with a median noise level of $2.7 \times 10^{-15} \text{ Hz}^{-1}$ measured at $T_{\text{det}} = 210$ mK. These numbers yield a NEP of $4 \times 10^{-18} \text{ W/Hz}^{0.5}$ at 1 Hz. For Device 2A, a responsivity of $1.2 \times$

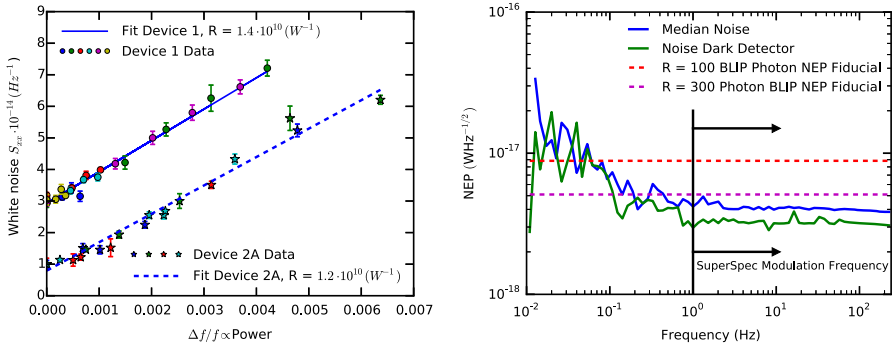


Fig. 2 Left: Measured responsivities for Devices 1 and 2A. Each different color symbol represents a different KID with resonant frequencies from 100 to 200 MHz. Coherent source was set to a frequency of 265 and 278 GHz, respectively. Detectors are assumed to have the same responsivity, and similarity of slopes between detectors confirms this assumption. Each detector for each device has been vertically offset to have the same Y-intercept. Right: NEP PSDs for SuperSpec detectors. NEP data shown are for Device 2A; however, absolute levels of the NEP curves are the same for both Device 1 and Device 2A. (Color figure online)

10^{10} W^{-1} (Fig. 2 left) is found along with a median noise value of $2.1 \times 10^{-15} \text{ Hz}^{-1}$, also yielding a NEP of $4 \times 10^{-18} \text{ W/Hz}^{0.5}$ at 1 Hz. Each SuperSpec die includes a KID which is not coupled to the filterbank as a way to assess chip-level effects. For this dark channel KID, the noise is slightly lower, $1.3 \times 10^{-15} \text{ Hz}^{-1}$, resulting in a detector NEP of $3 \times 10^{-18} \text{ W/Hz}^{0.5}$. The NEP measurements are shown in Fig. 2 right, and it can be seen that the device noise is below the expected photon noise level at the Large Millimeter Telescope (LMT). The instrument will be modulated with a chopping mirror for the LMT demonstration, and as such the low-frequency noise will not impact the sensitivity. For all devices, the T_c was approximately $\sim 0.93 \text{ K}$. As a result, these devices prefer to be operated at a lower T_{det} to reduce the thermal generation recombination (G-R) noise. This is demonstrated in the companion paper [8] where Device 1 was tested at lower T_{det} demonstrating even lower NEP can be achieved.

To determine the various contributions to the noise, noise is measured as a function of detector temperature (Fig. 3). At high detector temperatures, it is expected that thermal G-R noise becomes significant and dominates the noise levels, while at low temperatures photon noise is expected to come into play. This is supported by the observation that at low temperatures there is a correlation between efficiency on chip of each detector (measured by the fractional frequency response of each detector when exposed to a cold load at 77 K vs. a hot load at 300 K) and the white noise level, whereas at high detector temperatures this correlation disappears (Fig. 3 right). The fits to the noise levels are made using the formalism from [9] where $\tau_{qp} \sim (1 + n_{qp}/n^*)^{-1}$. Examining Fig. 3 left and the fits within reveals that the noise at the highest measured temperatures can be almost entirely attributed to thermal G-R noise. However, for the lowest temperature points, noise in excess of the thermal G-R noise for both the optical detectors and the dark channel KID on the optical chip is found. The ratio of the excess noise between the optical devices and the dark channel KID, approximately a factor of four, corresponds to the ratio of the response of these detectors to hot–cold

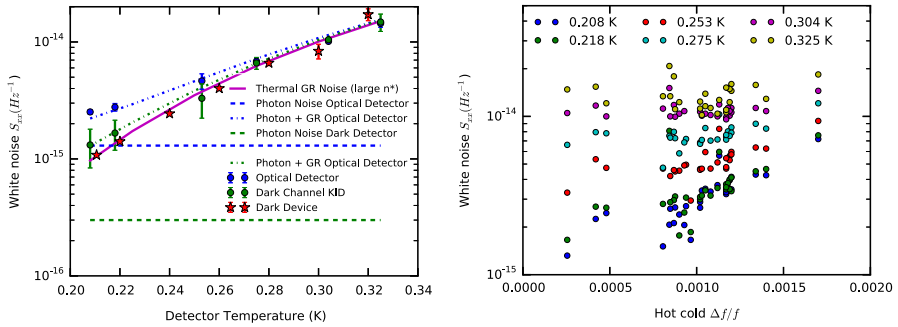


Fig. 3 Left: Noise versus detector temperature for SuperSpec Devices. Blue (typical optical channel) and green (dark channel) circles are for the optically coupled Device 2A, and the red stars are for Device 2B which was kept in a dark box. The fits to thermal G-R noise with and without a constant source of photon noise are also shown. Right: Noise as a function of the hot–cold response of Device 2A for different detector temperatures. (Color figure online)

loads outside the cryostat. Thus, this noise seems correlated to chip efficiency and is believed to be photon noise. It should be noted that the response of the dark channel is mostly contributed to by power below the spectral bank frequency range (the science band) but above the TiN band gap, that is 75–200 GHz. This is currently not filtered in the test bed, and for the telescope run, it will be mitigated by high-pass filtering. For Device 2B (the device in a dark package), the excess white noise is not seen at the lowest temperature and the noise can be entirely attributed to thermal G-R noise.

The instrument is expected to be strongly photon noise limited at the observatory because (a) loading from the coupling optics, telescope, and sky will be at least double the ~ 15 K level used here, and (b) further optimization of the system filtration and antenna/lens coupling are planned, increasing the efficiency of photons delivered to the detector.

3 Broadband Bow-tie Slot Antenna

SuperSpec employs a dual bow-tie slot antenna. The antenna consists of a microstrip-fed, dual-slot antenna, where the slots in the ground plane that make up the antenna have been flared out into a bow-tie shape. A scanning electron beam microscope image of the antenna is shown in Fig. 1b. Changing the previous dual-slot antenna to a dual bow-tie slot achieves a large bandwidth covering the entire 1-mm atmospheric window from 185 to 315 GHz, while maintaining simple lithography requirements. The antenna has a maximum length of 470 μm , and the slots are separated by a distance of 180 μm with a bow-tie flare angle of 34° . The antenna is coupled with a 5-mm-diameter hyperhemispherical silicon micro-lens. The design is optimized to work with a 1.25-mm extension length. The current test device has a 1.9-mm extension length which results in a few dB higher side-lobes and decreased efficiency. To determine the relative efficiency across the band, the response of a broadband detector on the feedline before the chip’s spectral channels to a Fourier transform spectrometer was measured. This is compared to the launching efficiency from ANSYS[®] HFSS[™] modeling in Fig. 4.

Fig. 4 Broadband antenna spectral response. Measured power has been normalized. The short-period fringing corresponds to a Fabry–Perot effect with a length scale that is roughly that of the separation between metal mesh filters in the cryostat. Telescope demonstration instrument will have optimized low-pass filtering as well as a 185-GHz high-pass filter. (Color figure online)

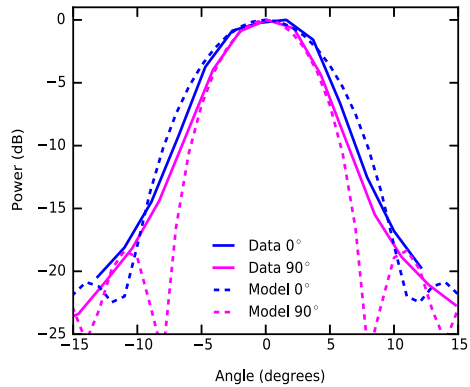
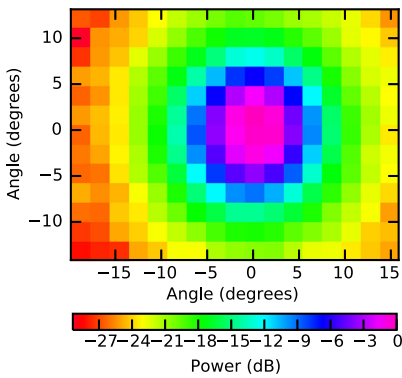
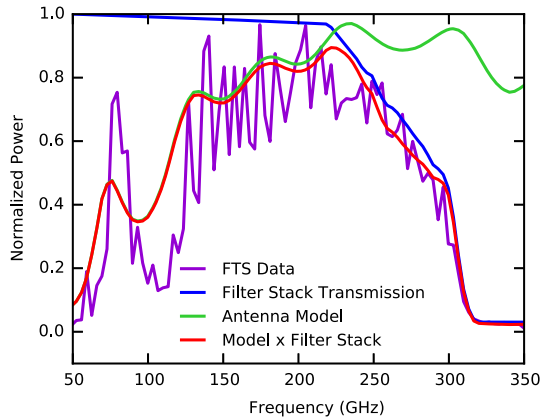


Fig. 5 Left: Beam map made from coadding all of the spectral channels’ beam responses. Right: Cuts of the beam map are compared with HFSS™ models. The spectral channels have an average frequency of 265 GHz, spanning a range 20 GHz, and the HFSS™ models were produced for the frequency of 265 GHz. (Color figure online)

When the filtering in the test bed is taken into account, good agreement between the measurements and the simulations is found.

Beam maps for the new antenna were performed by chopping a 77-K cold source against a 300-K background with a 1 inch aperture at a distance of 20 inches from the detector. At this distance, the measurements are in the far field of the lens and the antenna but not the far field of the limiting filter aperture at 4 K. This may cause some low-level beam distortion not captured by the models. The results of the beam maps are shown and compared with HFSS™ models in Fig. 5. Good agreement between the measurements and the models is found.

4 Conclusions

SuperSpec has achieved NEPs of $4 \times 10^{-18} \text{ W/Hz}^{0.5}$, ($3 \times 10^{-18} \text{ W/Hz}^{0.5}$ measured dark), meeting the photon-limited requirement for a $R = 300$ ground-based spec-

trometer for the best ground-based observing sites. For telescope loading levels, the on-telescope demonstration instrument should be strongly photon noise limited. A new broadband bow-tie slot antenna has been fabricated and demonstrated to achieve the necessary bandwidth to cover the entire 1-mm atmospheric window from 185 to 315 GHz. Additionally, the antenna produces the desired beam profiles at 265 GHz. In conclusion, SuperSpec prototypes have demonstrated that both the detectors and the optical coupling scheme meet the requirements for a SuperSpec demonstration instrument to be deployed on the Large Millimeter Telescope. This leads to the next step of designing, fabricating, and characterizing a full 300-channel spectrometer chip, of which the effort is currently underway.

Acknowledgements This work is supported in part by NASA Space Technology Research Fellowship NSTRF NNX15AQ09H and NSF AST ATI Grant 1407457.

References

1. J. Wheeler, S. Hailey-Dunsheath, E. Shirokoff, P.S. Barry, C.M. Bradford, S. Chapman, G. Che, J. Glenn, M. Hollister, A. Kovács, H.G. LeDuc, P. Mauskopf, R. McGeehan, C.M. McKenney, R. O'Brien, S. Padin, T. Reck, C. Rosset, C. Shiu, C.E. Tucker, R. Williamson, J. Zmuidzinis, *Proc. SPIE* (2016). <https://doi.org/10.1117/12.2233798>
2. S. Hailey-Dunsheath, E. Shirokoff, P.S. Barry, C.M. Bradford, S. Chapman, G. Che, J. Glenn, M. Hollister, A. Kovács, H.G. LeDuc, P. Mauskopf, C. McKenney, R. O'Brien, S. Padin, T. Reck, C. Shiu, C.E. Tucker, J. Wheeler, R. Williamson, J. Zmuidzinis, *J. Low Temp. Phys.* **84**, 180 (2016). <https://doi.org/10.1007/s10909-015-1375-x>
3. S. Hailey-Dunsheath, E. Shirokoff, P.S. Barry, C.M. Bradford, G. Chattopadhyay, P. Day, S. Doyle, M. Hollister, A. Kovács, H.G. LeDuc, P. Mauskopf, C.M. McKenney, R. Monroe, R. O'Brien, S. Padin, T. Reck, L. Swenson, C.E. Tucker, J. Zmuidzinis, *Proc. SPIE* (2014). <https://doi.org/10.1117/12.2057229>
4. A. Kovács, P.S. Barry, C.M. Bradford, G. Chattopadhyay, P. Day, S. Doyle, S. Hailey-Dunsheath, M. Hollister, C. McKenney, H.G. LeDuc, N. Llombart, D.P. Marrone, P. Mauskopf, R.C. O'Brien, S. Padin, L.J. Swenson, J. Zmuidzinis, *Proc. SPIE* **8452**, 84522G84522G10 (2012). <https://doi.org/10.1117/12.927160>
5. E. Shirokoff, P.S. Barry, C.M. Bradford, G. Chattopadhyay, P. Day, S. Doyle, S. Hailey-Dunsheath, M.I. Hollister, A. Kovács, C. McKenney, H.G. LeDuc, N. Llombart, D.P. Marrone, P. Mauskopf, R. O'Brien, S. Padin, T. Reck, L.J. Swenson, J. Zmuidzinis, *Proc. SPIE* (2012). <https://doi.org/10.1117/12.927070>
6. P.S. Barry, E. Shirokoff, A. Kovács, T.J. Reck, S. Hailey-Dunsheath, C.M. McKenney, L.J. Swenson, M.I. Hollister, H.G. LeDuc, S. Doyle, R. O'Brien, N. Llombart, D. Marrone, G. Chattopadhyay, P.K. Day, S. Padin, C.M. Bradford, P.D. Mauskopf, J. Zmuidzinis, *Proc. SPIE* (2012). <https://doi.org/10.1117/12.927089>
7. A.T. Crites, J.J. Bock, C.M. Bradford, T.C. Chang, A.R. Cooray, L. Duband, Y. Gong, S. Hailey-Dunsheath, J. Hunacek, P.M. Koch, C.T. Li, R.C. O'Brien, T. Prouve, E. Shirokoff, M.B. Silva, Z. Staniszewski, B. Uzgil, M. Zemcov, *Proc. SPIE* (2014). <https://doi.org/10.1117/12.2057207>
8. R. McGeehan, Noise performance of SuperSpec: an on-chip, TiN KID based mm-wave spectrometer. *J. Low Temp. Phys.* This Special Issue LTD17 (2018) (under review)
9. J. Zmuidzinis, *Annu. Rev. Condens. Matter Phys.* **3**(1), 169–214 (2012). <https://doi.org/10.1146/annurev-conmatphys-020911-125022>